nature COMMUNICATIONS

ARTICLE

Received 10 Oct 2012 | Accepted 15 Jan 2013 | Published 12 Feb 2013

DOI: 10.1038/ncomms2498

Electrical control of neutral and charged excitons in a monolayer semiconductor

Jason S. Ross[1,*], Sanfeng Wu[2,*], Hongyi Yu[3], Nirmal J. Ghimire[4,5], Aaron M. Jones[2], Grant Aivazian[2], Jiaqiang Yan[5,6], David G. Mandrus[4,5,6], Di Xiao[7], Wang Yao[3] & Xiaodong Xu[1,2]

Monolayer group-VI transition metal dichalcogenides have recently emerged as semiconducting alternatives to graphene in which the true two-dimensionality is expected to illuminate new semiconducting physics. Here we investigate excitons and trions (their singly charged counterparts), which have thus far been challenging to generate and control in the ultimate two-dimensional limit. Utilizing high-quality monolayer molybdenum diselenide, we report the unambiguous observation and electrostatic tunability of charging effects in positively charged (X^+), neutral (X^0) and negatively charged (X^-) excitons in field-effect transistors via photoluminescence. The trion charging energy is large (30 meV), enhanced by strong confinement and heavy effective masses, whereas the linewidth is narrow (5 meV) at temperatures <55 K. This is greater spectral contrast than in any known quasi-two-dimensional system. We also find the charging energies for X^+ and X^- to be nearly identical implying the same effective mass for electrons and holes.

[1] Department of Material Science and Engineering, University of Washington, Seattle, Washington 98195, USA. [2] Department of Physics, University of Washington, Seattle, Washington 98195, USA. [3] Department of Physics and Center of Theoretical and Computational Physics, University of Hong Kong, Hong Kong, China. [4] Department of Physics and Astronomy, University of Tennessee, Knoxville, Tennessee 37996, USA. [5] Materials Science and Technology Division, Oak Ridge National Laboratory, Oak Ridge, Tennessee 37831, USA. [6] Department of Materials Science and Engineering, University of Tennessee, Knoxville, Tennessee 37996, USA. [7] Department of Physics, Carnegie Mellon University, Pittsburgh, Pennsylvania 15213, USA. *These authors contributed equally to this work. Correspondence and requests for materials should be addressed to X.X. (e-mail: xuxd@uw.edu).

Above bandgap photo-excitation creates electrons and holes in the conduction and valence bands, respectively. If the screening is weak enough, the attractive Coulomb interaction between one electron and one hole creates a bound quasi-particle known as a neutral exciton (X^o), which has an energy structure similar to a neutral hydrogen atom. Excitons can further become charged by binding an additional electron (X^-) or hole (X^+) to form charged three-body excitons analogous to H^- or H_2^+ respectively[1–3]. These exciton species are elementary quasi-particles describing the electronic response to optical excitation in solids and are integral to many optoelectronic applications from solar cells and light-emitting diodes[4] to optical interconnects[5] and quantum logical devices[6,7].

The main arena for the exploration of excitonic physics has been three-dimensional semiconductors and their heterostructures that form quasi-2D quantum wells where the carrier wavefunction typically occupies a few tens to thousands of atomic layers. Observation and control of excitons in truly 2D systems has been a long pursued goal, largely motivated by the enhancement in exciton- and trion-binding energies in the strict 2D limit[8]. In addition, unlike semiconductor heterostructures, the close proximity of external stimuli to the exciton wavefunction can offer unprecedented tunability and diversifies the applications possible in devices made with 2D semiconductors.

Here we report the experimental observation and control of the fascinating excitonic physics in a 2D semiconductor by utilizing high-quality monolayer molybdenum diselenide ($MoSe_2$). $MoSe_2$ belongs to the group-VI transition metal dichalcogenides, which form in layers weakly bound to each other by Van der Waals forces. The monolayers have received much attention recently as they make up a new class of 2D semiconductors with a direct bandgap in the visible frequency range and are predicted to exhibit coupled spin-valley physics[9]. Recent progresses focus on MoS_2, including the demonstration of having a direct bandgap[10,11], high mobility electronics[12], optical generation of valley polarization[13–15] and electrical control of Berry phase properties[16].

Using a back-gated field-effect transistor (FET) device, we demonstrate the reversible electrostatic tunability of the exciton charging effects from positive (X^+) to neutral (X^o) and to negative (X^-). We observe a large trion-binding energy of 30 meV with a narrow emission linewidth of 5 meV. These narrow, well-separated features have temperature dependence of typical 2D excitons and exist at high temperature suggesting remarkable stability. Interestingly, the binding energies of X^+ and X^- are similar implying that low-energy electrons and holes in $MoSe_2$ have the same effective mass. Our work demonstrates that monolayer $MoSe_2$ is a true 2D semiconductor opening the door for the investigation of phenomena such as exciton condensation[17–19] and the Fermi-edge singularity[20,21], as well as for a new generation of optoelectronic devices such as light-emitting diodes and excitonic circuits[5].

Results

Crystal structure and spectral features of monolayer $MoSe_2$. In monolayer $MoSe_2$, Mo and Se atoms form a 2D hexagonal lattice with trigonal prismatic coordination (Fig. 1a). First-principles calculations show that it has a direct bandgap at the corners (K points) of the first Brillouin zone (Fig. 1b). The curvature of the bands suggests comparable effective mass for low-energy electrons and holes at K points (Fig. 1c)[9]. These band-edge electrons and holes near K points are predominantly from the *d*-orbitals of Mo atoms. Their wavefunctions are calculated to be strongly confined in the Mo layer within a length scale of ~0.2 nm in the out-of-plane direction. Monolayer $MoSe_2$ is thus an ideal nanomaterial for exploring excitonic physics in the ultimate 2D limit.

We use mechanical exfoliation to obtain monolayer $MoSe_2$ on 300 nm SiO_2 on n^+-doped Si and atomic force microscope to

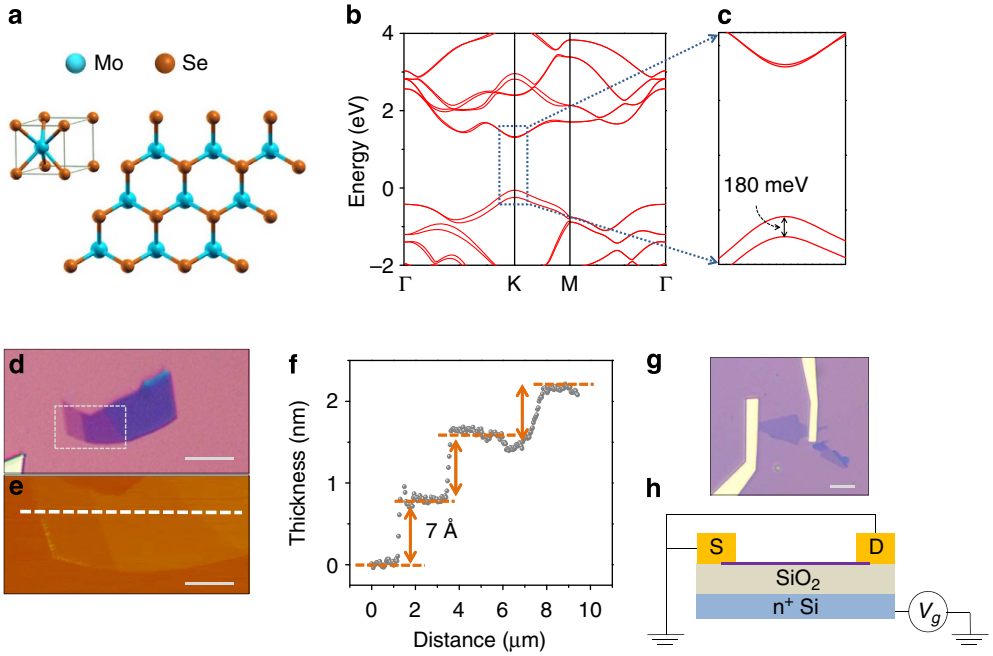

Figure 1 | $MoSe_2$ characteristics and devices. (**a**) Coordination structure and top view of monolayer $MoSe_2$. (**b**) Density function theory calculated band structure. (**c**) Band structure at K point shows 180 meV valence band splitting due to spin–orbit coupling. (**d**) Optical micrograph of exfoliated $MoSe_2$ flake on 300 nm SiO_2. Scale bar, 5 μm. (**e**) atomic force microscope (AFM) image of area highlighted in (**d**). Scale bar, 1 μm. (**f**) AFM line scan along dashed line in **e**. (**g**) Optical micrograph of $MoSe_2$ device. Scale bar, 5 μm. (**h**) Schematic of back-gated $MoSe_2$ device.

identify the layer thickness[22]. Figure 1d,e show the optical micrograph and the corresponding atomic force microscope image of a representative sample, in which the monolayer thickness of ~0.7 nm is identified[12] (Fig. 1f). Standard electron beam lithography (EBL) is used to fabricate monolayer FETs (Fig. 1g). With the contacts simply grounded, the n^+ Si functions as a back gate providing uniform electrostatic doping in the $MoSe_2$ (Fig. 1h).

The excitonic features of $MoSe_2$ are investigated by differential reflectance and micro photoluminescence (PL) measurements (Methods). Figure 2 shows the results from an unpatterned $MoSe_2$ sample, S1. At 20 K, we observe two main features associated with the A and B excitons in the differential reflection spectrum[10,11,14,23–25] (Fig. 2a). The presence of A and B excitons has been attributed to spin–orbit coupling-induced valence band splitting in bulk[24]. The observed energy difference of ~200 meV agrees well with the calculated splitting (180 meV) in monolayers (Fig. 1c).

With the same sample and temperature under 2.33 eV laser excitation, the PL spectrum does not show a measurable feature that can be attributed to the B exciton, likely because it is not the lowest energy transition. Instead, we observe two pronounced peaks at 1.659 and 1.627 eV in the vicinity of the A exciton (Fig. 2b). Note that the PL spectrum lacks the broad low-energy peak observed in MoS_2, which has been attributed to defect-related, trapped exciton states[10,11,14,25].

The striking spectral features demonstrate the high quality of our $MoSe_2$ samples (Methods) and provide strong evidence for monolayer $MoSe_2$ being a direct bandgap semiconductor (Supplementary Fig. S1) where the two distinct transitions are excitons. The higher-energy emission at 1.659 eV is the neutral exciton, X^o, and the lower-energy peak is a trion[3]. In unpatterned samples, we assume the trion to be X^- because all measured devices show n-doped characteristics (Supplementary Fig. S2). All measured unpatterned samples show a binding energy, which is the energy difference between trion and X^o, of ~30 meV (Fig. 2b, inset). This is more than twice the typical numbers reported in GaAs quantum wells[3,26,27] and similar to a recent mention in MoS_2[14].

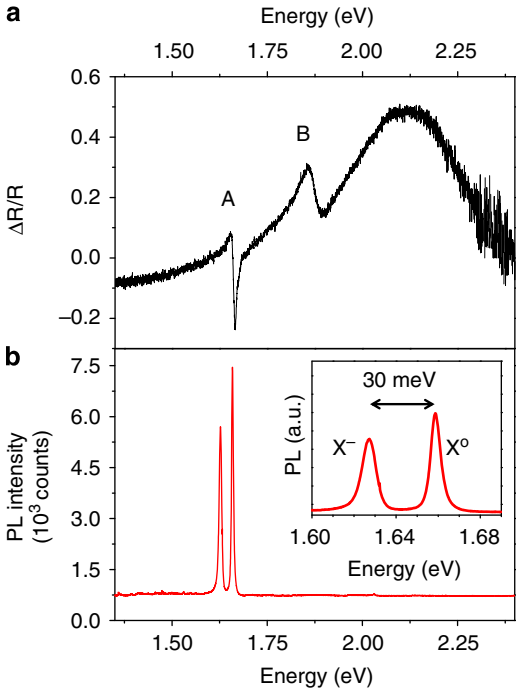

Figure 2 | Differential reflectance and PL spectra of monolayer $MoSe_2$ at 20 K. (**a**) Differential reflectance shows A and B excitons. (**b**) PL excited by 2.33 eV laser shows neutral exciton (X^o) and the lower-energy charged exciton (X^-). PL from the B exciton has not been observed. Inset, PL of the exciton peaks. The X^- shows a binding energy of about 30 meV.

Gate dependence of $MoSe_2$ PL. To confirm the above assignment and control the exciton charging effects, we performed gate-dependent PL measurements using monolayer $MoSe_2$ FETs. Here the excitation laser is at 1.73 eV for better resonance with the luminescent states. Figure 3a shows a colour map of the PL spectrum of device D1 at 30 K as a function of back-gate voltage, V_g, in which we clearly observe four spectral features whose intensities strongly depend on V_g. Near zero V_g, the spectrum shows a broad low-energy feature around 1.57 eV and a narrow high-energy peak at 1.647 eV. With large V_g of either sign, these peaks disappear and a single-emission peak dominates the spectrum. Both peaks (at negative or positive V_g) have similar energies and intensities with the latter increasing with the magnitude of V_g.

This observed gate dependence confirms the assignment of states as labelled in Fig. 3a. Because the broad low-energy peak does not show up in unpatterned samples before FET fabrication, we attribute it to exciton states trapped to impurities (X^I)[10,11,14,25], which are likely introduced during EBL processing and are not the focus of this paper. The sharp peak at 1.647 eV is the X^o, slightly red-shifted compared with unpatterned samples. From the gate dependence, we identify the peaks near 1.627 eV as the X^- and X^+ trions when V_g is largely positive and negative, respectively. Remarkably, these two distinct quasi-particles (X^+ and X^-) exhibit a nearly identical binding energy. The difference is within 1.5 meV over the whole applied V_g range. Because the binding energy of a trion is dependent on its effective mass, this observation implies that the electron and hole have approximately the same effective mass.

The gate-dependent measurements unambiguously demonstrate the electrical control of exciton species in a truly 2D semiconductor, as illustrated in Fig. 3b. The conversion from X^o to trion can be represented as $e(h) + X^o \rightarrow X^-$ (X^+), where e and h represent an electron or a hole, respectively. By setting V_g to be negative, the sample is p-doped, favouring excitons to form lower-energy-bound complexes with free holes. As V_g decreases, more holes are injected into the sample, and all X^o turn into X^+ to form a positively charged hole-trion gas. With positive V_g, a similar situation occurs with free electrons to form an electron-trion gas. In the following, we show that a standard mass action model can be used to describe the conversion dynamics.

Figure 3c shows the extracted X^o (black) and trion (red) peak intensity as a function of V_g where we have adjusted the negative V_g data due to background signal. The plot shows that the maximum X^o intensity is about equal to the saturated trion PL when X^o vanishes. This observation indicates conservation of the total number of X^o and trion in the applied voltage range and similar radiative decay rates for both quasi-particles. Thus, the PL intensity represents the amount of the corresponding exciton species. Because the dynamic equilibrium of free electrons, holes and excitons are governed by the rate equation and law of mass action[27], we calculate the gate-dependent X^o and trion abundance (Supplementary Fig. S3), shown by the solid lines in Fig. 3c, which agrees with the data.

In the simulation, we first fit the X^o curve to obtain our two free parameters: the maximum background electron concentration $n_B^{max} = 3.6 \times 10^{10} cm^{-2}$ when the trion intensity saturates and the photo-excited electron concentration $n_p = 1.5 \times 10^{10} cm^{-2}$. We then fit the trion gate dependence

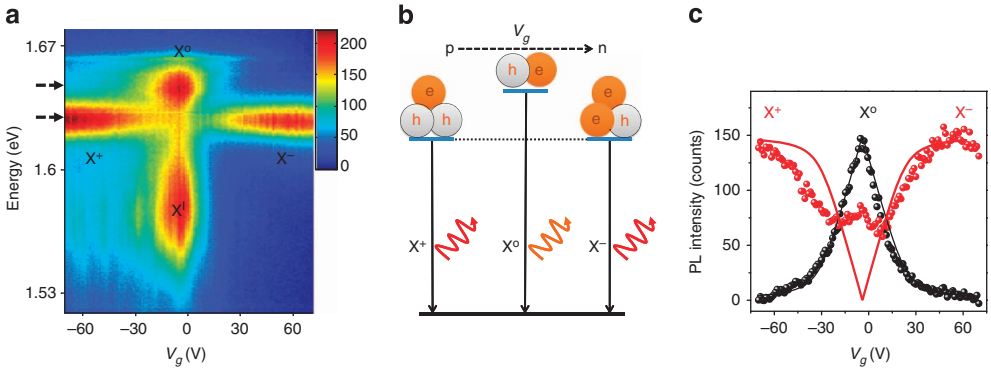

Figure 3 | Electrostatic control of exciton charge. (**a**) $MoSe_2$ PL (colour scale in counts) is plotted as a function of back-gate voltage. Near zero doping, we observe mostly neutral and impurity-trapped excitons. With large electron (hole) doping, negatively (positively) charged excitons dominate the spectrum. (**b**) Illustration of the gate-dependent trion and exciton quasi-particles and transitions. (**c**) Trion and exciton peak intensity versus gate voltage at dashed arrows in (**a**). Solid lines are fits based on the mass action model.

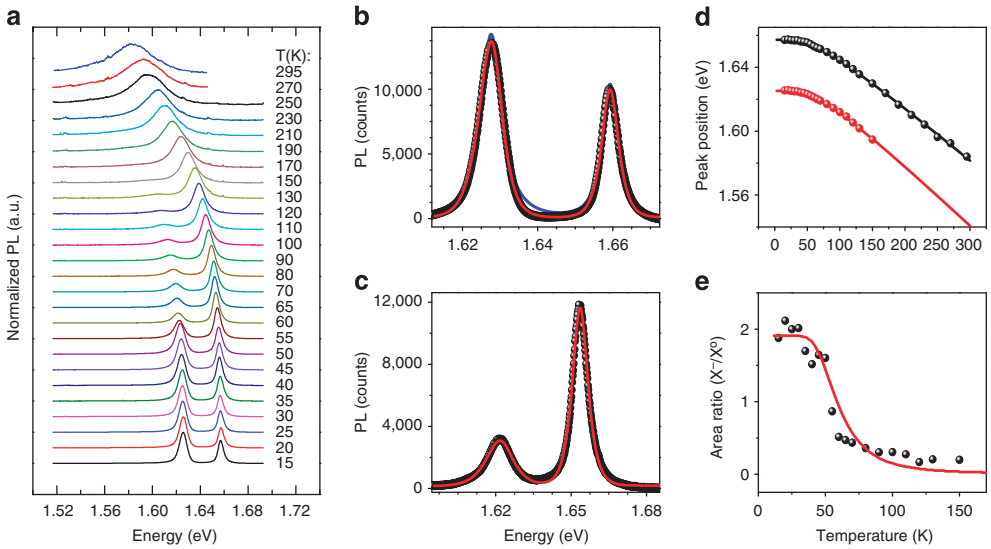

Figure 4 | Temperature dependence of PL spectrum. (**a**) Normalized PL of monolayer $MoSe_2$ versus temperature. (**b**) Line shape fitting at 15 K. Black is data. Red and blue curves are fits with and without considering the electron-recoil effect, respectively. (**c**) Data and fit at 70 K using two symmetric peaks. (**d**) Neutral exciton (black) and trion (red) peak position versus temperature with fits (solid lines). (**e**) Integrated area ratio of trion:exciton versus temperature with mass action model fitting (red).

with these parameters held fixed (Supplementary Note 1). The deviation in the trion experimental data from the calculated curve near zero V_g is artificial due to the mutual background from X^o and X^I. We note that this inferred electron concentration is much smaller than the product of the gate capacitance and V_g. This discrepancy can be attributed to the large contact resistance (Supplementary Fig. S4) of the sample, which prevents the carrier concentration from reaching equilibrium on the experimental time scale at 30 K. We expect that future improved contact technologies will eliminate this effect.

Temperature dependence of $MoSe_2$ PL. The observed exciton states also show fine features consistent with 2D excitons, such as temperature-dependent line shape, peak energy and relative weight of X^o and trion, which further supports the excitonic nature of this monolayer system (Fig. 4). Figure 4a shows the evolution of X^- and X^o (normalized PL) as a function of temperature in an unpatterned sample, S2, under 1.96 eV laser excitation. At low temperatures, we again observe a binding energy of 30 meV. As the temperature rises, we see the X^- signal drop significantly at about 55 K, which we attribute to electrons escaping their bound trion state due to thermal fluctuations (Supplementary Note 1).

Figure 4b is the zoom-in plot at 15 K where we observe slightly different line shapes for X^- and X^o. The X^o peak is symmetric showing homogenous thermal broadening effects and is well fit by a hyperbolic secant function that yields a full-width half-maximum of 5 meV[27,28]. However, the X^- peak shows a slightly asymmetric profile with a long low-energy tail consistent with electron-recoil effects[27]. The recombination of a X^- with momentum k will emit a photon and leave a free electron with the same momentum k due to momentum conservation. From energy conservation, the emitted photon has an energy $\hbar\omega = \hbar\omega_o - \frac{\hbar k^2}{2m_e^*}\frac{M_{X^o}}{M_{X^-}}$, where $\hbar\omega_o$ is the energy of trions with $k=0$, and M_{X^o} and M_{X^-} are the X^o and X^- effective masses, respectively. The line shape of trion PL will thus be the convolution of a symmetric peak function (hyperbolic secant) and an exponential low-energy tail function (Supplementary Fig. S5 and Supplementary Note 2). When the temperature is >70 K,

we find that homogenous broadening dominates over electron recoil and the PL spectrum is fit well by two hyperbolic secant functions (Fig. 4c).

From the fits, we extract the X^- and X^o peak position (Fig. 4d) and the ratio of the integrated intensity of the X^- to the X^o (Fig. 4e) where we do not present trion data >150 K because it becomes negligible. We find that the peak positions are fit well (solid line in Fig. 4d) using a standard semiconductor bandgap dependence[29] of $E_g(T) = E_g(0) - S\hbar\omega\left[\coth\left(\frac{\hbar\omega}{2kT}\right) - 1\right]$, where $E_g(0)$ is the ground-state transition energy at 0 K, S is a dimensionless coupling constant and $\hbar\omega$ is an average phonon energy. From the fits, we extract for X^o (X^-) the $E_g = 1.657$ (1.625) eV, $S = 1.96$ (2.24) and $\hbar\omega = 15$ meV for both. Applying our mass action model (Supplementary Fig. S3 and Supplementary Note 1) with a trion-binding energy of 30 meV results in a good fit to the X^-:X^o intensity ratio (solid line in Fig. 4e).

Discussion

In summary, we have shown that monolayer $MoSe_2$ is a true 2D excitonic system, which exhibits strong electrostatic tuning of exciton charging via a standard back-gated FET. The observed narrow, well-separated spectral features are within the titanium (Ti)-Sapphire laser spectral range and thus provide remarkable opportunities to selectively probe and control specific excitons using current continuous wave and ultrafast Ti-Sapphire laser technologies. Our results further demonstrate that high-quality monolayer dichalcogenides can serve as a platform for investigating excitonic physics and photonic applications in the truly 2D limit with the potential to outperform quasi-2D systems. The results represent unique prospects for this burgeoning class of 2D materials, in addition to the recent attention received for their valley physics. Our work expands the horizons for using 2D semiconductors for diverse fundamental studies and technical applications.

Note: During the review process, we became aware of the independent observation of negatively charged exciton in monolayer MoS_2 (ref. 30) and investigation of PL intensity of thin-film $MoSe_2$ as a function of temperature[31].

Methods

Sample growth. $MoSe_2$ single crystals were grown by vapour transport. First, $MoSe_2$ powder was prepared by heating a stoichiometric mixture of Mo (Alfa, 99.999%) powder and Se (Alfa, 99.999%) pieces sealed in a quartz tube under 1/3 atmosphere of pure argon. The ampoule was slowly heated up to 850 °C and kept at this temperature for 24 h. Then, 3.5 g of $MoSe_2$ powder was mixed with 0.5 g of iodine and sealed in a quartz tube. The sealed ampoule was loaded into a tube furnace for 10 days, with the hot zone kept at 1,050 °C and the growth zone at 1,000 °C. Plate-like crystals with typical dimensions $6 \times 10 \times 0.1$ mm^3 were obtained at the cold end. Room-temperature X-ray diffraction confirmed that the samples are single phase with 2H structure. Elemental analysis was performed using a Hitachi TM-3000 tabletop electron microscope equipped with a Bruker Quantax 70 energy-dispersive X-ray system. The analysis confirmed the expected stoichiometric Mo:Se ratio in the crystals.

Device fabrication. After mechanical exfoliation of $MoSe_2$ monolayers on SiO2 substrates, a JEOL JBX-6300FS EBL system was used to pattern contacts in a 300-nm bilayer PMMA resist. An e-beam evaporator was used to deposit 6/60 nm of Ti/Au followed by liftoff in hot acetone, cleaning in several IPA baths and drying under N2.

Optical measurements. All spectra were collected via a Princeton Instruments Acton 2500i grating spectrometer and an Andor Newton CCD (charge-coupled device), with samples in a helium-flow cryostat. For differential reflectance measurements, an Ocean Optics tungsten halogen white light source is reflected into a $\times 40$ ultra-long working distance objective using a neutral density, achromatic beam splitter and then focused on the sample ($\sim 2\,\mu$m spot size). The reflected signal from the sample is collected by the objective and sent back through the beam splitter into the spectrometer. For PL measurements, a similar setup is used, except the neutral density beam splitter is replaced by a dichroic beam splitter appropriate for the laser wavelength and a laser line notch filter is inserted before the spectrometer.

References

1. Lampert, M. Mobile and immobile effective-mass-particle complexes in nonmetallic solids. *Phys. Rev. Lett.* **1,** 450–453 (1958).
2. Finkelstein, G., Shtrikman, H. & Bar-Joseph, I. Negatively and positively charged excitons in GaAs/$Al_xGa_{1-x}As$ quantum wells. *Phys. Rev. B* **53,** R1709–R1712 (1996).
3. Kheng, K., Cox, R. & D'Aubigné, M. Observation of negatively charged excitons X^- in semiconductor quantum wells. *Phys. Rev. Lett.* **71,** 1752–1755 (1993).
4. Scholes, G. D. & Rumbles, G. Excitons in nanoscale systems. *Nat. Mater.* **5,** 683–696 (2006).
5. High, A. A., Novitskaya, E. E., Butov, L. V., Hanson, M. & Gossard, A. C. Control of exciton fluxes in an excitonic integrated circuit. *Science* **321,** 229–231 (2008).
6. Carter, S. G. *et al.* Quantum coherence in an optical modulator. *Science* **310,** 651–653 (2005).
7. Kira, M., Koch, S. W., Smith, R. P., Hunter, A. E. & Cundiff, S. T. Quantum spectroscopy with Schrödinger-cat states. *Nat. Phys.* **7,** 799–804 (2011).
8. Stébé, B. & Ainane, A. Ground state energy and optical absorption of excitonic trions in two dimensional semiconductors. *Superlattice. Microstruct.* **5,** 545–548 (1989).
9. Xiao, D., Liu, G.-B., Feng, W., Xu, X. & Yao, W. Coupled spin and valley physics in monolayers of MoS_2 and other group-VI dichalcogenides. *Phys. Rev. Lett.* **108,** 1–5 (2012).
10. Splendiani, A. *et al.* Emerging photoluminescence in monolayer MoS_2. *Nano. Lett.* **10,** 1271–1275 (2010).
11. Mak, K., Lee, C., Hone, J., Shan, J. & Heinz, T. Atomically thin MoS_2: a new direct-gap semiconductor. *Phys. Rev. Lett.* **105,** 2–5 (2010).
12. Radisavljevic, B., Radenovic, A., Brivio, J., Giacometti, V. & Kis, A. Single-layer MoS_2 transistors. *Nat. Nanotechnol.* **6,** 147–150 (2011).
13. Cao, T. *et al.* Valley-selective circular dichroism of monolayer molybdenum disulphide. *Nat. Commun.* **3,** 887 (2012).
14. Mak, K. F., He, K., Shan, J. & Heinz, T. F. Control of valley polarization in monolayer MoS_2 by optical helicity. *Nat. Nanotechnol.* **7,** 494–498 (2012).
15. Zeng, H., Dai, J., Yao, W., Xiao, D. & Cui, X. Valley polarization in MoS2 monolayers by optical pumping. *Nat. Nanotechnol.* **7,** 490–493 (2012).
16. Wu, S. *et al.* Electrical tuning of valley magnetic moment through symmetry control in bilayer MoS_2. *Nat. Phys.* doi:10.1038/NPHYS2524 (2013).
17. Eisenstein, J. P. & Macdonald, A. H. Bose–Einstein condensation of excitons in bilayer electron systems. *Nature* **432,** 691–694 (2004).
18. Butov, L. V., Gossard, A. C. & Chemla, D. S. Macroscopically ordered state in an exciton system. *Nature* **418,** 751–754 (2002).
19. Deng, H. & Yamamoto, Y. Exciton-polariton Bose–Einstein condensation. *Rev. Mod. Phys.* **82,** 1489–1537 (2010).
20. Chen, W. *et al.* Excitonic enhancement of the Fermi-edge singularity in a dense two-dimensional electron gas. *Phys. Rev. B* **45,** 8464–8477 (1992).
21. Finkelstein, G., Shtrikman, H. & Bar-Joseph, I. Optical spectroscopy of a two-dimensional electron gas near the metal-insulator transition. *Phys. Rev. Lett.* **74,** 976–979 (1995).
22. Novoselov, K. S. *et al.* Two-dimensional atomic crystals. *Proc. Natl Acad. Sci. USA* **102,** 10451–10453 (2005).
23. Evans, B. L. & Hazelwood, R. A. Optical and structural properties of $MoSe_2$. *Physica Status Solidi (a)* **4,** 181–192 (1971).
24. Coehoorn, R., Haas, C. & De Groot, R. Electronic structure of $MoSe_2$, MoS_2, and WSe_2. II. The nature of the optical band gaps. *Phys. Rev. B* **35,** 6203–6206 (1987).
25. Korn, T., Heydrich, S., Hirmer, M., Schmutzler, J. & Schuüller, C. Low-temperature photocarrier dynamics in monolayer MoS_2. *Appl. Phys. Lett.* **99,** 102109 (2011).
26. Warburton, R. *et al.* Optical emission from a charge-tunable quantum ring. *Nature* **405,** 926–929 (2000).
27. Esser, A., Runge, E. & Zimmermann, R. Photoluminescence and radiative lifetime of trions in GaAs quantum wells. *Phys. Rev. B* **62,** 8232–8239 (2000).
28. Esser, A., Runge, E., Zimmermann, R. & Langbein, W. Trions in GaAs quantum wells: photoluminescence lineshape analysis. *Physica Status Solidi (a)* **178,** 489–494 (2000).
29. O'Donnell, K. P. & Chen, X. Temperature dependence of semiconductor band gaps. *Appl. Phys. Lett.* **58,** 2924–2926 (1991).
30. Mak, K. F. *et al.* Tightly bound trions in monolayer MoS2. *Nat. Mater.* doi:10.1038/nmat3505 (2012).
31. Tongay, S. *et al.* Thermally driven crossover from indirect toward direct bandgap in 2D semiconductors: MoSe2 versus MoS2. *Nano Lett.* **12,** 5576–5580 (2012).

Acknowledgements

We thank David Cobden and Ming Gong for their helpful discussions. This work is mainly supported by the US DoE, BES, Materials Sciences and Engineering Division (DE-SC0008145). H.Y. and W.Y. were supported by Research Grant Council of Hong Kong (HKU706412P). N.J.G., J.Y., D.G.M. and D.X. were supported by the US DoE, BES, Materials Sciences and Engineering Division. Device fabrication was

performed at the University of Washington Microfabrication Facility and NSF-funded Nanotech User Facility.

Author contribution

X.X. conceived the experiments. J.S.R. fabricated the devices and performed the measurements, assisted by S.W., A.M.J. and G.A. S.W., J.S.R. and X.X. performed data analysis. H.Y., W.Y. and D.X. contributed to the theoretical explanation. N.G., J.Y. and D.G.M. synthesized and performed bulk characterization measurements on the $MoSe_2$ crystals. All authors discussed the results and contributed to writing the manuscript.

Additional information

Supplementary Information accompanies this paper at http://www.nature.com/naturecommunications

Competing financial interests: The authors declare no competing financial interests.

Reprints and permission information is available online at http://npg.nature.com/reprintsandpermissions/

How to cite this article: Ross, J.S. *et al.* Electrical control of neutral and charged excitons in a monolayer semiconductor. *Nat. Commun.* 4:1474 doi: 10.1038/ncomms2498 (2013).

nature materials

LETTERS

PUBLISHED ONLINE: 2 DECEMBER 2012 | DOI: 10.1038/NMAT3505

Tightly bound trions in monolayer MoS_2

Kin Fai Mak[1], Keliang He[2], Changgu Lee[3], Gwan Hyoung Lee[4], James Hone[4], Tony F. Heinz[1] and Jie Shan[2]*

Two-dimensional (2D) atomic crystals, such as graphene and transition-metal dichalcogenides, have emerged as a new class of materials with remarkable physical properties[1]. In contrast to graphene, monolayer MoS_2 is a non-centrosymmetric material with a direct energy gap[2–5]. Strong photoluminescence[2,3], a current on/off ratio exceeding 10^8 in field-effect transistors[6], and efficient valley and spin control by optical helicity[7–9] have recently been demonstrated in this material. Here we report the spectroscopic identification in a monolayer MoS_2 field-effect transistor of tightly bound negative trions, a quasiparticle composed of two electrons and a hole. These quasiparticles, which can be optically created with valley and spin polarized holes, have no analogue in conventional semiconductors. They also possess a large binding energy (~20 meV), rendering them significant even at room temperature. Our results open up possibilities both for fundamental studies of many-body interactions and for optoelectronic and valleytronic applications in 2D atomic crystals.

The trion binding energy that we observe in monolayer MoS_2 is nearly an order of magnitude larger than that found in conventional quasi-2D systems, such as semiconductor quantum wells[10–13]. This is a consequence of the greatly enhanced Coulomb interactions in monolayer MoS_2, arising from reduced dielectric screening in gapped 2D crystals and the relatively heavy particle band masses associated with the Mo d-manifolds[4,5,14]. For an electron density as high as $n = 10^{11}$ cm^{-2}, for instance, the dimensionless interaction parameter r_s is ~60 in monolayer MoS_2 (Supplementary Section S1). This value is significantly larger than that for carriers in quantum wells even at very low doping levels[15]. Monolayer MoS_2 is a strongly interacting system even in the presence of relatively high carrier densities; it thus presents an ideal laboratory for exploring many-body phenomena, such as carrier multiplication and Wigner crystallization[16].

The atomic structure of MoS_2 consists of hexagonal planes of S and Mo atoms in a trigonal prismatic structure (Fig. 1a; ref. 17). The two sublattices of the hexagonal MoS_2 structure are occupied, respectively, by one Mo and two S atoms (Fig. 1b). Monolayer MoS_2 is a direct gap semiconductor with energy gaps located at the K and K′ points of the Brillouin zone (Fig. 1c). Both the highest valence bands and the lowest conduction bands are formed primarily from the Mo d-orbitals[4,17]. The large spin–orbit interaction splits the highest valence bands at the K (K′) point by ~160 meV (refs 2,3,7). The valley and spin degrees are coupled because of the lack of inversion symmetry in monolayer MoS_2 (ref. 18). As has been recently shown experimentally, this allows optical pumping of a single valley (and spin) with circularly polarized light[7–9].

Here we investigate the optical response of monolayer MoS_2 as a function of carrier density by means of absorption and photoluminescence spectroscopy. In our investigations we have made use of MoS_2 monolayers prepared by mechanical exfoliation. Field-effect transistors (FETs) using MoS_2 were fabricated on SiO_2/Si substrates; the doping density in the MoS_2 channel was systematically varied by applying a voltage to the Si back gate. All measurements were performed at 10 K, if not otherwise specified. The typical variation of the drain–source current (I_{ds}) with the gate voltage (V_g) is shown in the inset of Fig. 1d. The response is characteristic of a FET with an n-type channel. Spontaneous negative doping, presumably from defects within the MoS_2 layer and/or substrate interactions, has been commonly reported in mechanically exfoliated MoS_2 (refs 6,19). Over the accessible range of the gate voltage (−100 to +80 V) our MoS_2 FETs exhibit electron doping. The low off-state current at high negative gate voltages is understood to reflect electron localization in 2D (ref. 15) and/or a channel-contact barrier.

The absorption spectrum of monolayer MoS_2 at a gate voltage of −100 V (Fig. 1d) corresponds to that of a nearly undoped sample. It shows pronounced absorption peaks from excitonic transitions, rather than the steps that would be expected for absorption arising from band-to-band transitions in 2D. The two features, known as the A (~1.92 eV) and B (~2.08 eV) excitons[2,3,20], are associated with direct optical transitions from the highest spin-split valence bands to the lowest conduction bands. These transitions are significantly modified by strong Coulomb interactions between the photogenerated electron–hole pairs and the corresponding formation of bound excitons.

In our investigation of the optical response of MoS_2 in the presence of a 2D electron gas (2DEG), we focus on the behaviour of the low-energy (A) exciton over the spectral range of 1.8–2.0 eV. Figure 2a (red lines) shows representative absorption spectra of a monolayer MoS_2 FET under gate voltages from −100 to 80 V, corresponding to approximate charge neutrality to a doping density of ~ 10^{13} cm^{-2}. We see an overall suppression of the optical absorbance in this spectral region with increasing electron doping. The prominent A exciton peak evolves into two resonances, with the emergence of a lower energy resonance (labelled as A$^-$). For $V_g > 0$, the absorbance of feature A diminishes rapidly and disappears into the background. The A$^-$ feature, on the other hand, broadens gradually, while approximately preserving its spectral weight. Similarly, in the photoluminescence spectra (Fig. 2a), both resonances can be identified for negative gate voltages. The photoluminescence intensity of the A exciton, like its absorbance, can be switched off by doping. In addition, redshifts in the photoluminescence peak energies from the corresponding absorption energies (Stokes shifts) are observed for both features; the magnitude of Stokes shift is found to increase with doping level (Supplementary Fig. S1b).

[1]Departments of Physics and Electrical Engineering, Columbia University, 538 West 120th Street, New York 10027, USA, [2]Department of Physics, Case Western Reserve University, 10900 Euclid Avenue, Cleveland, Ohio 44106, USA, [3]SKKU Advanced Institute of Nanotechnology (SAINT) and Department of Mechanical Engineering, Sungkyunkwan University, Suwon 440-746, Korea, [4]Department of Mechanical Engineering, Columbia University, New York 10027, USA. *e-mail: jie.shan@case.edu.

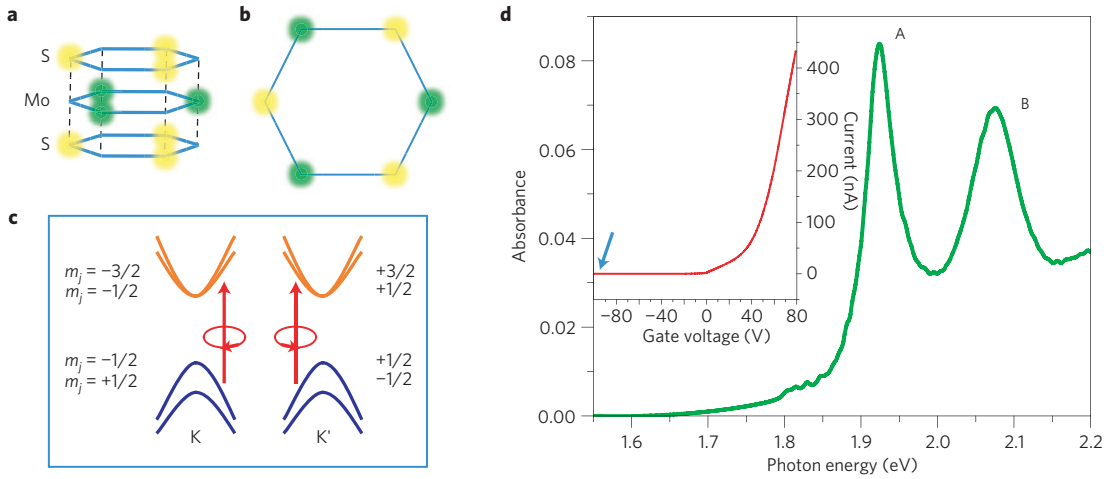

Figure 1 | Atomic structure, electronic band structure, and absorption spectrum of monolayer MoS_2. a, Representation of the trigonal prismatic structure of monolayer MoS_2. **b**, Honeycomb lattice structure with each sublattice occupied by a Mo and two S atoms. **c**, The lowest-energy conduction bands and the highest-energy valence bands labelled by the *z*-component of their total angular momentum near the K and K′ point of the Brillouin zone. The spin degeneracy at the valence-band edges is lifted by spin–orbit interactions. The valley and spin degrees of freedom are coupled. Under left-circularly polarized excitation, only the K-valley is populated, whereas under right-circularly polarized excitation, only the K′-valley is populated. **d**, Absorption spectrum of undoped monolayer MoS_2 with two prominent resonances, known as the A and B excitons. The inset shows the drain–source current I_{ds}, under a $V_{ds} = 40$ mV bias voltage, as a function of back-gate voltage V_g. It is characteristic of an *n*-doped semiconductor that can be turned off at large negative gate voltages.

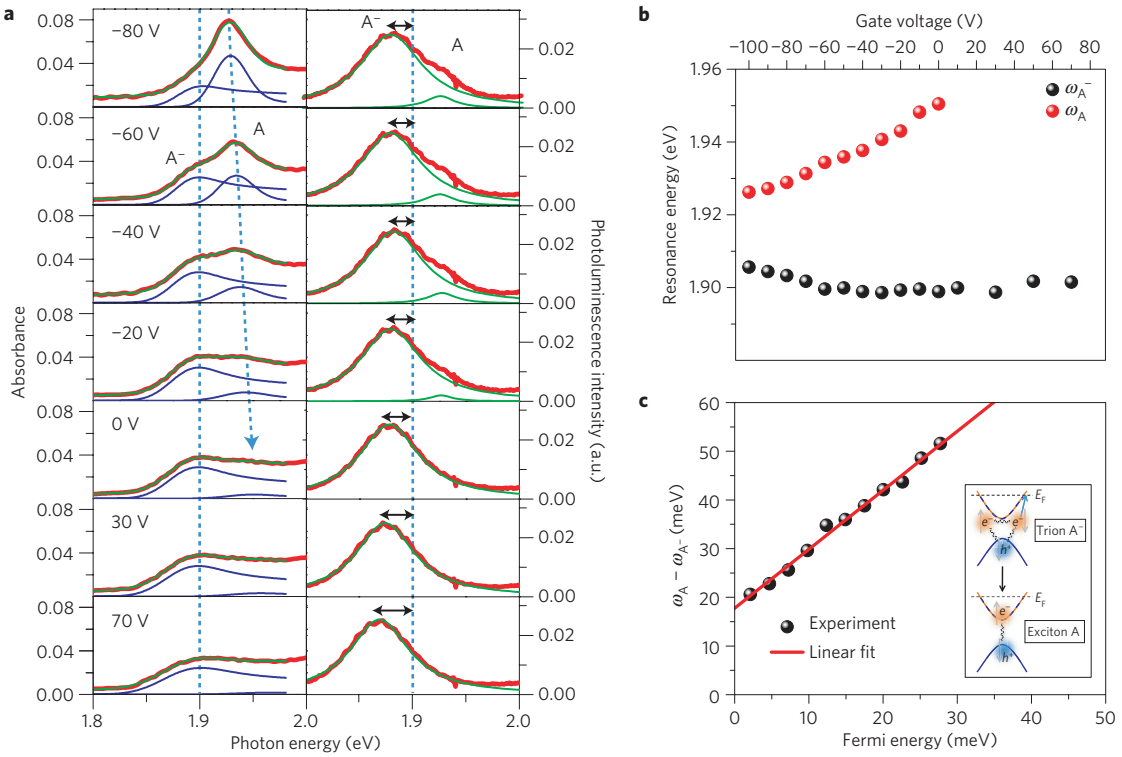

Figure 2 | Doping dependence of the optical properties of a monolayer MoS_2 FET. a, Absorption and photoluminescence spectra (red lines) in the range of 1.8–2.0 eV for the indicated back-gate voltages. The exciton (A) and trion (A^-) resonances behave differently with gate voltage. Left: Absorption spectra, with the dashed blue lines as a guide to the eye for the threshold energies of A and A^- features. The green lines are power-law fits to the experimental results, as described in the main text, with the A and A^- components shown as the blue lines. Right: The photoluminescence spectra of the A and A^- features are fit to Lorentzians (green lines). The dashed blue line indicates the absorption peak of the A^- resonance and the arrows show the doping-dependent Stokes shift of the trion photoluminescence. **b**, Threshold energies of the trion ω_{A^-} (black symbols) and the neutral exciton ω_A (red symbols), determined from the absorption spectra, as a function of gate voltage (upper axis) and Fermi energy E_F (lower axis). **c**, The difference in the exciton and trion energies, $\omega_A - \omega_{A^-}$ (symbols), as a function of Fermi energy E_F. The red line, a linear fit to the E_F-dependence, has a slope of 1.2 and an intercept of 18 meV. The latter determines the trion binding energy. Inset: representation of the dissociation of a trion into an exciton and an electron at the Fermi level.

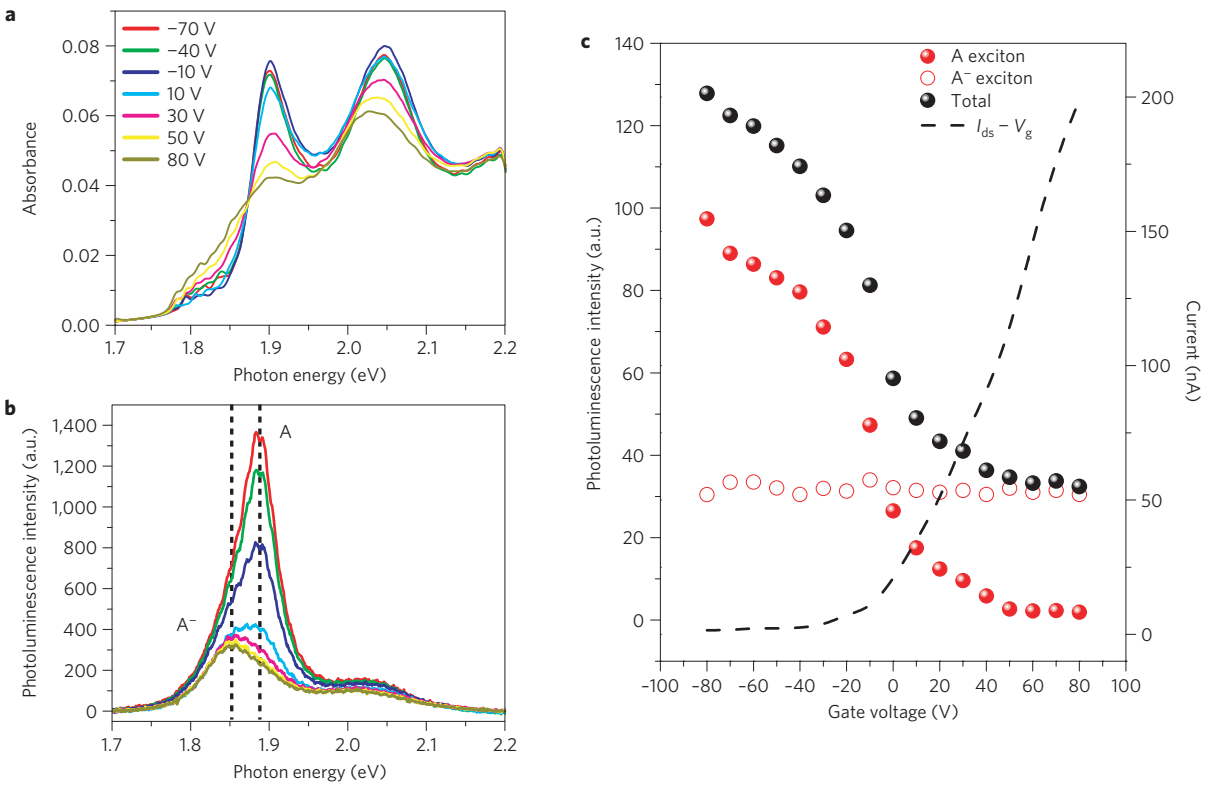

Figure 3 | Excitons and trions at room temperature in monolayer MoS_2. a,**b**, Absorption and photoluminescence spectra at different back-gate voltages. Both the neutral exciton (A) and trion (A^-) features (with the corresponding resonance energies indicated by the dashed lines) can be identified, although the resonances are significantly broadened. **c**, Dependence on gate voltage of the drain–source current (right) and the integrated photoluminescence intensity of the A and A^- features and their total contribution (left).

What is the origin of the A^- resonance? Our observation cannot be explained by a simple state-blocking effect. Although such Pauli blocking can account for the overall reduction in absorption with doping[21], it cannot explain the appearance of two resonances with different doping dependences. Nor can the emergence of two features be explained by an electric-field-induced band structure modification. In the absence of magnetic fields, the valley and spin degeneracy of the bands is protected and no available degeneracy can be lifted to give rise to two distinct resonances. The observed A^- feature, however, can be understood as arising from trions. Such bound states of two electrons to a hole, that is, negatively charged excitons, are known to have finite binding energies[10,11,22,23]. In our experiment at low temperature, the optical response of monolayer MoS_2 is dominated by neutral excitons in undoped samples. Trions emerge, accompanied by a reduction of exciton absorption and photoluminescence, when excess electrons are introduced to bind to photoexcited electron–hole pairs. The exciton spectral weight is transferred to the trion, as shown in our experiment. The detailed dependence on doping density of this phenomenon in the relatively low doping regime is often governed by electron localization in inhomogeneous samples.

We have analysed the absorption spectra to determine the energies to create both neutral excitons (ω_A) and trions (ω_{A^-}) as a function of the doping level. The analysis is based on a fitting procedure using the predicted power-law spectral dependence[21,24] of the features (see Methods for details)[21,24]. We also convert the gate voltage to the electron doping density ($ne = CV_g$) using the back-gate capacitance of $C = 1.2 \times 10^{-8}\,\mathrm{F\,cm^{-2}}$ and then to the Fermi energy ($E_F = \hbar^2\pi n/2m_e e^2$) using an electron band mass of $m_e = 0.35m_0$ (ref. 14), where m_0 is the electron mass. Because of intrinsic charging effects, we furthermore introduce an offset in the gate voltage of $-107 \pm 6\,\mathrm{V}$ for $E_F = 0$. This value was extrapolated from the gate dependence of the photoluminescence Stokes shift[21,25] (Supplementary Section S2).

When the Fermi energy is varied from ~0 to 30 meV, the exciton energy blue-shifts monotonically, whereas the trion energy remains largely unchanged, after a slight initial redshift (Fig. 2b). These dependences arise from the combined effects of Pauli blocking and many-body interactions[25,26], and are consistent with the previous theoretical results (Supplementary Section S3) and experimental studies on quantum wells (refs 10–13). The splitting between the exciton and trion energy is predicted to be linearly dependent on the Fermi energy and obey[11]

$$\omega_A - \omega_{A^-} = E_{A^-} + E_F \quad (1)$$

where E_{A^-} is the trion binding energy. Because the exciton can be considered as an ionized trion, $\omega_A - \omega_{A^-}$ defines the minimum energy for the removal of one electron from the trion. In the limit of infinitesimal doping, it is just the trion binding energy E_{A^-}, the energy required to promote one of the electrons in a trion to the conduction band edge. At finite doping densities, an exciton is obtained by dissociation of a trion and placing the extra electron at the Fermi level, all lower conduction band levels being occupied at zero temperature (inset of Fig. 2c). Our experimental result for $\omega_A - \omega_{A^-}$ agrees very well with equation (1) (Fig. 2c), further confirming the spectroscopic assignment of the exciton and trion features. We also determine the trion binding energy from the linear fit to be $18.0 \pm 1.5\,\mathrm{meV}$. This value is compatible with an estimated trion binding energy of $E_{A^-} \sim 0.1E_A$ (for isotropic 2D semiconductors with equal electron and hole masses[23]) and the calculated exciton binding energy of $E_A \approx 0.6\,\mathrm{eV}$ (refs 14,27).

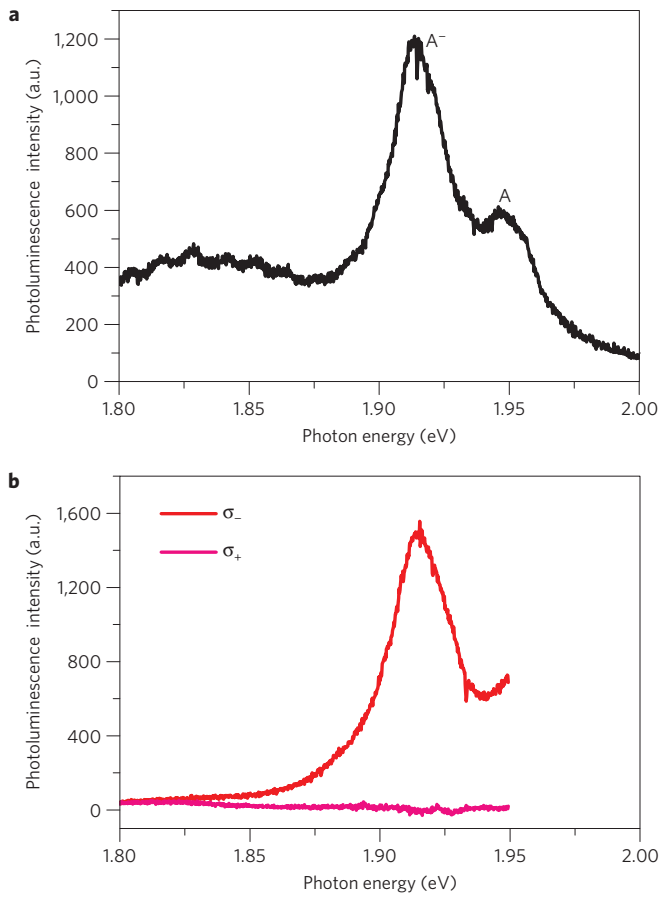

Figure 4 | Valley and spin control of trions in monolayer MoS_2. **a**, Photoluminescence spectrum of a monolayer MoS_2 sample on a h-BN substrate at 10 K with fully resolved exciton (A) and trion (A^-) emission. **b**, The left-circularly polarized (σ_-) and right-circularly polarized (σ_+) component of the trion emission for excitation by σ_- light at 1.96 eV, nearly on-resonance with the A exciton.

The large trion binding energy observed in monolayer MoS_2 suggests the importance of trions even at elevated temperatures. Indeed, both the exciton and trion features can be identified in the optical response of doped monolayer MoS_2 at room temperature (Fig. 3a,b), although the resonances are significantly broadened. The absorption and especially photoluminescence are highly dependent on doping (Fig. 3c). Whereas the trion photoluminescence is largely gate independent, the exciton photoluminescence varies by nearly two orders of magnitude, which is also correlated with the $I_{ds} - V_g$ dependence[12]. This dependence arises primarily from a spectral weight reduction of the exciton resonance with doping, which is consistent with the low-temperature data (although less noticeable at low doping levels owing to the finite temperature effects). The tuning range of the exciton photoluminescence could be further increased with better quality samples. Such strong tunability of the exciton photoluminescence was not observed at 10 K, where emission originates from hot photoluminescence before exciton–trion equilibrium is reached, whereas at room temperature, exciton photoluminescence originates primarily from populations thermally excited from the trion state.

Finally, we demonstrate the unique spin and valley properties of trions in monolayer MoS_2. Figure 4a shows the photoluminescence spectrum for a monolayer MoS_2 sample on a hexagonal boron nitride (h-BN) substrate at 10 K, where the trion and exciton features are fully resolved because of the high homogeneity of the sample. We optically pump the sample at 1.96 eV, nearly on-resonance with the A exciton, by left-circularly polarized light (σ_-). The trion emission is found to be nearly 100% of the same helicity as the pump light (Fig. 4b). Whereas the optical selection rules dictate a single exciton state with hole spin up and electron spin down in the K-valley on absorption of a σ_- photon, multiple trion states are allowed. Among them the lowest energy state consists of hole spin up and two electrons spin down in the K-valley when valley and spin exchange interactions are included. Our photoluminescence result indicates that the optically excited hole in the trion remains spin up, that is, in the K-valley (for a time much longer than the trion lifetime), even in the presence of strong exchange mediated spin relaxation. This suggests the robustness of the hole valley index as a result of the coupled valley and spin degree of freedom[18,22].

The existence of tightly bound trions with dynamically controllable hole valley and spin in monolayer MoS_2 opens up possibilities of novel many-body phenomena. The large trion binding energy in 2D atomic crystals may also impact the development of new photonic and optoelectronic devices, such as optical detectors or photovoltaic cells. In contrast to neutral excitons, trions can be guided by electric fields, suggesting schemes to overcome the losses associated with the usual diffusive motion of neutral excitons.

Methods

Sample preparation. Monolayer MoS_2 samples were mechanically exfoliated from bulk MoS_2 crystals (SPI) on silicon substrates covered by a 280 nm layer of thermal oxide. Monolayer samples, typically of an area $>50\,\mu m^2$, were identified by optical microscopy. The sample thickness was confirmed independently by atomic-force microscopy and photoluminescence measurements[2,13]. Monolayer MoS_2 FET devices were fabricated by defining drain and source contacts either through e-beam lithography or photolithography, followed by deposition of Cr/Au or Ni in an e-beam evaporator. For the polarization resolved measurement, the exfoliated samples were transferred to hexagonal boron nitride substrates.

Optical measurements. Monolayer MoS_2 FETs were first characterized at 10 K and at room temperature when the back gate was varied systematically from −100 to 80 V. No significant hysteresis was observed. The drain–source current I_{ds} was measured in the linear response regime under a drain–source bias voltage $V_{ds} = 40$ mV across a channel length of 10 μm. For optical absorption measurements, the broadband radiation from a quartz tungsten halogen source was focused onto monolayer MoS_2 by a 40× objective. The reflected radiation was collected and analysed with a grating spectrometer equipped with a liquid nitrogen cooled CCD.

The reflectance contrast was measured by normalizing the radiation reflected from the sample on substrate to that from the bare substrate. The sample absorbance was obtained from the reflectance by using a Kramers–Kronig constrained variational analysis[28] (Supplementary Section S4). Photoluminescence measurements were performed using the same set-up with a single-mode solid-state laser centred at 532 nm. The laser intensity on the sample was kept below 500 W cm^{-2}, which corresponds to a steady-state photoexcitation density of $\sim 10^{10}$ cm^{-2} in monolayer MoS_2 (refs 2,29). This is ∼2–3 orders of magnitude lower than the electron doping density induced by the silicon back gate. For the polarization resolved measurements, a Babinet–Soleil compensator was used to produce circularly polarized 632.8 nm light from a HeNe laser. Emission from the sample passed through a combination of a quarter-wave Fresnel rhomb and an analyser for selection of the left- and right-circularly polarized components.

Analysis of the absorption spectra. We used the predicted single-sided power-law spectral dependence of the exciton and trion absorbance in doped 2D semiconductors, $A(\omega) = \Sigma_{X=A,A^{-1}} a_X(\omega - \omega_X)^{-\alpha_X}$ (for $\omega > \omega_X$) (refs 21,24). This expression corresponds to a shake-up process, a non-instantaneous evolution of the 2DEG to a new equilibrium configuration on creation of a hole[21,24]. Here a_X, ω_X and α_X are, respectively, the amplitude, threshold energy and critical exponent of resonance X (= A and A^-). In the limit of relatively low doping densities, as in our experiment, a_X ($X = A, A^-$) depend weakly on doping[24] and were kept as constants. To compare with experiment, the power-law dependence was convoluted with a Gaussian to account for sample inhomogeneity and the onset of indirect optical transitions in doped semiconductors[21]. In addition, a smooth background describing the low-energy tail of higher energy transitions was subtracted from experimental spectra. (See Supplementary Sections S3 and S4 for details.) The fits (green lines, Fig. 2a), with individual contributions from excitons and trions (blue lines), are in good agreement with experiment (red lines). At positive gate voltages the exciton absorption is very weak and is omitted from the fitting.

Received 23 July 2012; accepted 30 October 2012; published online 2 December 2012

References

1. Novoselov, K. S. Nobel lecture: Graphene: Materials in the Flatland. *Rev. Mod. Phys.* **83,** 837–849 (2011).
2. Mak, K. F., Lee, C., Hone, J., Shan, J. & Heinz, T. F. Atomically thin MoS_2: A new direct-gap semiconductor. *Phys. Rev. Lett.* **105,** 136805 (2010).
3. Splendiani, A. *et al.* Emerging photoluminescence in monolayer MoS_2. *Nano Lett.* **10,** 1271–1275 (2010).
4. Li, T. & Galli, G. Electronic properties of MoS_2 nanoparticles. *J. Phys. Chem. C* **111,** 16192–16196 (2007).
5. Lebegue, S. & Eriksson, O. Electronic structure of two-dimensional crystals from *ab initio* theory. *Phys. Rev. B* **79,** 115409 (2009).
6. Radisavljevic, B., Radenovic, A., Brivio, J., Giacometti, V. & Kis, A. Single-layer MoS_2 transistors. *Nature Nanotech.* **6,** 147–150 (2011).
7. Mak, K. F., He, K., Shan, J. & Heinz, T. F. Control of valley polarization in monolayer MoS_2 by optical helicity. *Nature Nanotech.* **7,** 494–498 (2012).
8. Zeng, H., Dai, J., Yao, W., Xiao, D. & Cui, X. Valley polarization in MoS_2 monolayers by optical pumping. *Nature Nanotech.* **7,** 490–493 (2012).
9. Cao, T. *et al.* Valley-selective circular dichroism of monolayer molybdenum disulphide. *Nature Commun.* **3,** 887 (2012).
10. Kheng, K. *et al.* Observation of negatively charged excitons X^- in semiconductor quantum wells. *Phys. Rev. Lett.* **71,** 1752–1755 (1993).
11. Huard, V., Cox, R. T., Saminadayar, K., Arnoult, A. & Tatarenko, S. Bound states in optical absorption of semiconductor quantum wells containing a two-dimensional electron gas. *Phys. Rev. Lett.* **84,** 187–190 (2000).
12. Finkelstein, G., Shtrikman, H. & Bar-Joseph, I. Optical spectroscopy of a two-dimensional electron gas near the metal-insulator transition. *Phys. Rev. Lett.* **74,** 976–979 (1995).
13. Lee, C. *et al.* Anomalous lattice vibrations of single- and few-layer MoS_2. *ACS Nano* **4,** 2695–2700 (2010).
14. Cheiwchanchamnangij, T. & Lambrecht, W. R. L. Quasiparticle band structure calculation of monolayer, bilayer, and bulk MoS_2. *Phys. Rev. B* **85,** 205302 (2012).
15. Spivak, B., Kravchenko, S. V., Kivelson, S. A. & Gao, X. P. A. Colloquium: Transport in strongly correlated two dimensional electron fluids. *Rev. Mod. Phys.* **82,** 1743–1766 (2010).
16. Wigner, E. On the interaction of electrons in metals. *Phys. Rev.* **46,** 1002–1011 (1934).
17. Mattheiss, L. F. Band structures of transition-metal-dichalcogenide layer compounds. *Phys. Rev. B* **8,** 3719–3740 (1973).
18. Xiao, D., Liu, G-B., Feng, W., Xu, X. & Yao, W. Coupled spin and valley physics in monolayers of MoS_2 and other group-VI dichalcogenides. *Phys. Rev. Lett.* **108,** 196802 (2012).
19. Ayari, A., Cobas, E., Ogundadegbe, O. & Fuhrer, M. S. Realization and electrical characterization of ultrathin crystals of layered transition-metal dichalcogenides. *J. Appl. Phys.* **101,** 014507 (2007).
20. Evans, B. L. & Young, P. A. Optical absorption and dispersion in molybdenum disulphide. *Proc. R. Soc. Lond. A* **284,** 402 (1965).
21. Ruckenstein, A. E. & Schmitt-Rink, S. Many-body aspects of the optical spectra of bulk and low-dimensional doped semiconductors. *Phys. Rev. B* **35,** 7551–7557 (1987).
22. Stebe, B. & Ainane, A. Ground-state energy and optical-absorption of excitonic trions in two-dimensional semiconductors. *Superlattices Microstruct.* **5,** 545–548 (1989).
23. Thilagam, A. Two-dimensional charged-exciton complexes. *Phys. Rev. B* **55,** 7804–7808 (1997).
24. Ohtaka, K. & Tanabe, Y. Theory of the soft-X-ray edge problem in simple metals: Historical survey and recent developments. *Rev. Mod. Phys.* **62,** 929–991 (1990).
25. Hawrylak, P. Optical properties of a two-dimensional electron gas: Evolution of spectra from excitons to Fermi-edge singularities. *Phys. Rev. B* **44,** 3821–3828 (1991).
26. Ogawa, T. Quantum states and optical responses of low-dimensional electron-hole systems. *J. Phys. Condens. Matter* **16,** S3567–S3595 (2004).
27. Ramasubramaniam, A. Large excitonic effects in monolayers of molybdenum and tungsten dichalcogenides. *Phys. Rev. B* **86,** 115409 (2012).
28. Kuzmenko, A. B. Kramers-Kronig constrained variational analysis of optical spectra. *Rev. Scient. Inst.* **76,** 083108 (2005).
29. Korn, T., Heydrich, S., Hirmer, M., Schmutzler, J. & Schueller, C. Low-temperature photocarrier dynamics in monolayer MoS_2. *Appl. Phys. Lett.* **99,** 102109 (2011).

Acknowledgements

This research was supported by the National Science Foundation through grants DMR-0907477 and the Research Corporation Scialog Program at Case Western Reserve University; and by the National Science Foundation through grants DMR-1106172 and 1122594 and by the Department of Energy, Office of Basic Energy Sciences through grant DE-FG02-07ER15842 at Columbia University and through grant DE-SC0001085 for optical instrumentation at Columbia University's Center for Re-Defining Photovoltaic Efficiency through Molecule Scale Control. C.L. acknowledges support from the Korean government Ministry of Education grant Global Frontier Research Center for Advanced Soft Electronics (2011-0031629), and G.H.L. support from Samsung-SKKU Graphene Center.

Author contributions

K.F.M. and J.S. designed the experiment, performed the measurement and analysis, and prepared the manuscript; K.H. fabricated MoS_2 FET devices and measured photoluminescence; C.L. and J.H. developed MoS_2 FET devices; G.H.L fabricated MoS_2 samples on BN; T.F.H. contributed to the interpretation of the results and writing of the manuscript.

Additional information

Supplementary information is available in the online version of the paper. Reprints and permissions information is available online at www.nature.com/reprints. Correspondence and requests for materials should be addressed to J.S.

Competing financial interests

The authors declare no competing financial interests.